Energy Storage Materials 45 (2022) 821–827

Contents lists available at ScienceDirect

Energy Storage Materials

journal homepage: www.elsevier.com/locate/ensm

Spinel-related $Li_2Ni_{0.5}Mn_{1.5}O_4$ cathode for 5-V anode-free lithium metal batteries

Liangdong Lin[a], Kun Qin[a], Meiying Li[a], Yong-sheng Hu[a], Hong Li[a], Xuejie Huang[a], Liquan Chen[a], Liumin Suo[a,b,c,*]

[a] Beijing Advanced Innovation Center for Materials Genome Engineering, Key Laboratory for Renewable Energy, Beijing Key Laboratory for New Energy Material and Devices, Beijing National Laboratory for Condensed Matter Physics, Institute of Physics, Chinese Academy of Science, Beijing 100190, China
[b] Center of Materials Science and Optoelectronics Engineering, University of Chinese Academy of Sciences, Beijing 100049, China
[c] Yangtze River Delta Physics Research Center Co. Ltd, Liyang 213300, China

ARTICLE INFO

Keywords:
Li-rich
Spinel-related
Anode-free
Lithium metal batteries
Lithium metal anodes

ABSTRACT

The anode-free lithium metal battery with high voltage $LiNi_{0.5}Mn_{1.5}O_4$ cathode is an excellent Co-free high energy density (ED) system. However, it suffers severely from cycling capacity fading due to no lithium compensation from the anode side. In this study, as against $LiNi_{0.5}Mn_{1.5}O_4$ cathode, Li-rich $Li_2Ni_{0.5}Mn_{1.5}O_4$ is proposed, which can smoothly convert into $LiNi_{0.5}Mn_{1.5}O_4$ and release a large amount of Li-ions at the first charge to replace the Li loss in the following cycle, thereby extending the lifespan of the battery without the introduction of inactive components. Using such a Li-rich cathode, the anode-free pouch cell attained 367-Wh kg^{-1} stack ED and 88% capacity retention (CR) after 50 cycles, with limited electrolyte addition (E/C ratio of 2 g Ah^{-1}). Our work provides a new low-cost strategy to explore high ED Co-free Li metal batteries.

1. Introduction

The application of Li-ion batteries has significantly grown with the expansion of electric vehicles, electric energy storage, and the internet of things [1–3], which also drives the considerable demand for Co resources. To address the Co resource restriction issue, a low-Co or even Co-free cathode alternative was investigated [4–7]. Considering cost and energy density (ED), high voltage Co-free spinel $LiNi_{0.5}Mn_{1.5}O_4$ (LNMO) is one of the most promising candidates yet to be commercialized (Tab. S1) [8–16]. Since LNMO cathode provides Li resources, the anode-free design is suitable for increasing the ED of the LNMO full-cell while reducing material costs [17–21]. Directly pairing the LNMO cathode with a bare Cu current collector makes the anode-free Li metal battery (AF-LMB) advantageous in cell fabrication compared with traditional Li-ion batteries (LIBs), with graphite as the anode or LMBs, with metallic Li foil as the anode. First, without applying the anode materials onto the current collector, the preparation of the anode is excluded. Second, the low-dew-point environment required to operate highly reactive metallic Li is unnecessary.

Despite that, the capacity of the lithium metal anode (LMA) fades fasts, with comparable low Coulombic efficiency (CE) [22,23]. The virtually infinite volume change, potential dendrite growth, and dead Li generation during Li plating/stripping fail to form a robust solid electrolyte interphase (SEI), leading to a continuous side-reaction, consuming the reversible Li resources [24–28]. Thus, the challenge for anode-free LMBs lie in achieving a long cycling life without excessive Li compensation (Li foil) at the anode side since any irreversible loss of Li will directly decrease the capacity. To address the above issue, various strategies have been attempted to improve the CE of the LMA to ~99.7%, including functional electrolytes [9,29-31], interface engineering [32,33], and robust hosts [34]. However, side-reactions between Li and the electrolyte are still completely unavoidable. Assuming a CE of 99.7%, the capacity retentions (CRs) of AF-LMBs are < 74% after 100 cycles, which is unacceptable for real applications (> 80%). Thus, the Li foil on the anode side, as a compromise, is used to offset the Li loss. However, the use of a thick Li foil leads to severe ED loss, whereas an ultrathin Li foil is inconvenient. Therefore, using the extra Li resources inside the Li-rich cathode (Li_2 $[Ni_{0.8}Co_{0.1}Mn_{0.1}]O_4$) to increase the cycle life of AF-LMBs without the introduction of troublesome metallic Li is promising [35]. Although such cell design can achieve high ED, a large demand for Co-free batteries in many price-sensitive markets still exists.

Here, a similar strategy of using a Li-rich cathode to extend the lifespan of AF-LMB is introduced into the LNMO cell by replacing LNMO cathode with Li-rich $Li_2Ni_{0.5}Mn_{1.5}O_4$ (L_2NMO) [8,36]. L_2NMO is a spinel-related phase, which evolves from spinel LNMO through Li intercalation. Compared with conventional LNMO, ~twice as many Li-ions

* Corresponding author.
E-mail address: suoliumin@iphy.ac.cn (L. Suo).

https://doi.org/10.1016/j.ensm.2021.12.036
Received 11 August 2021; Received in revised form 7 December 2021; Accepted 24 December 2021
Available online 26 December 2021

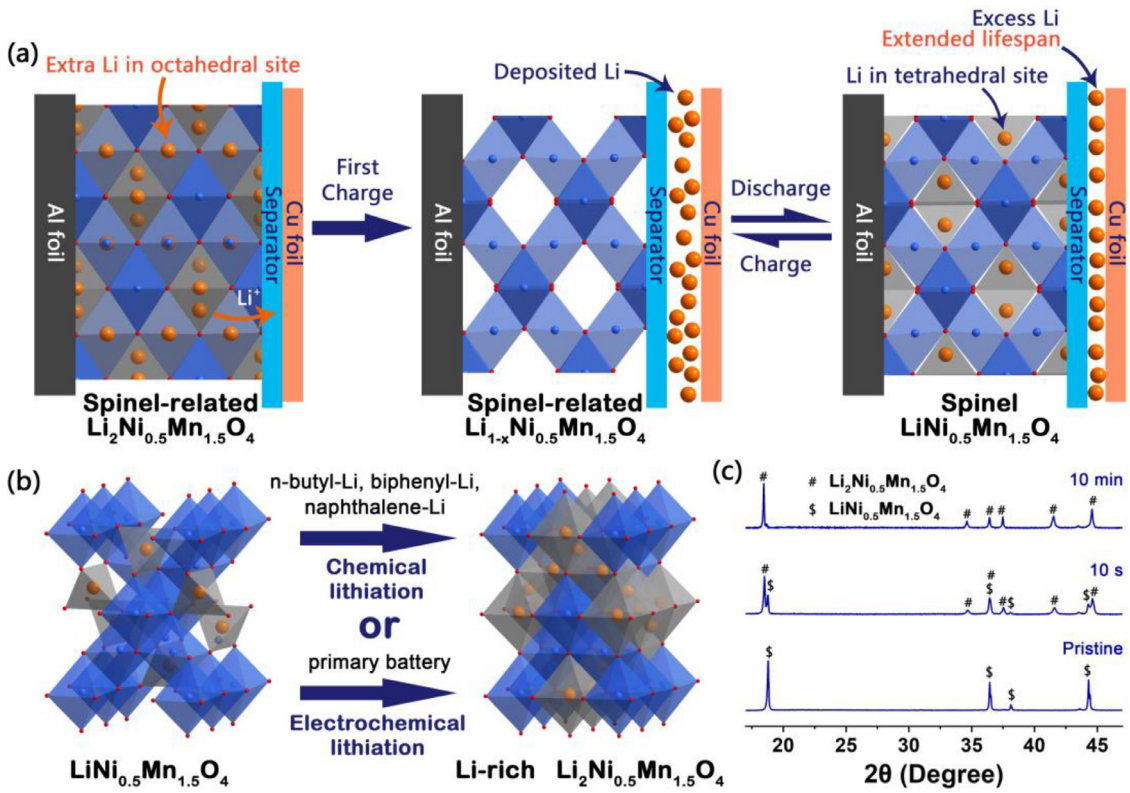

Fig. 1. Concept of $Li_2Ni_{0.5}Mn_{1.5}O_4$ (L_2NMO) based anode-free Li metal battery. (a) Schematic representation of the L_2NMO extending the lifespan of AF-LMB. (b) Schematic illustration of L_2NMO synthesized by chemical lithiation or electrochemical lithiation. (c) XRD patterns of LNMO react with n-butyl Li for different periods.

can intercalate into the unoccupied octahedral sites of LNMO to form L_2NMO without affecting the occupation of preexisting tetrahedral Li-ions and octahedral transition metal ions (Fig. 1a). The L_2NMO can be reversibly converted to the conventional LNMO by de-intercalating excess Li from the octahedral sites during the first charging process, which will be temporarily stored in the anode as a Li reservoir (Fig. 1a). Notably, after Li supplementation, L_2NMO can continuously participate in cell cycling function as an LNMO cathode active material without introducing inactive components, thus improving the lifespan of AF-LMB without sacrificing its ED, which is undoubtedly more advanced than some pre-lithiation additives [37–44]. More importantly, the fabrication of such AF-LMB is safer without the highly reactive metallic Li. All these factors make this concept attractive for developing low-cost batteries with considerable ED.

The preparations of partially lithiated LNMO ($Li_{1+x}Ni_{0.5}Mn_{1.5}O_4$ (L_{1+x}NMO), $0 < x < 1$) using microwave-assisted chemical lithiation [45], coprecipitation followed by two thermal treatments [46–48], liquid ammonia chemical lithiation [49], and over-discharge of LNMO half-cell [8,48], have been reported. However, in these studies, the full-cells only used LNMO with lithiation degrees < 70% as cathodes and Si/C, graphite, or FeSb/TiC as anodes, resulting in non-pronounced EDs and CRs. Here fully lithiated L_2NMO is prepared by chemical lithiation of $P4_332$ type LNMO (Fig. 1b) and applied to AF-LMB with increased ED and CR. For instance, the reaction between n-butyl Li and LNMO at room temperature can produce L_2NMO (Fig. 1c). LNMO can be completely lithiated in only 10 min, confirmed by the disappearance of LNMO reflections (Fig. 1c) and inductively coupled plasma-optical emission spectrometry (ICP-OES, Tab. S2). Furthermore, other lithiation agents are also successfully demonstrated to lithiate LNMO into L_2NMO (Fig. S1, S2), as well as the electrochemical lithiation methods using Li metal as the anode (Fig. S3, S4). Using the L_2NMO as a cathode, the anode-free pouch cell we assembled with high cathode mass loading (25 mg cm^{-2}) and limited electrolyte addition (E/C ratio of 2 g Ah^{-1}). The high CR of 88% after 50 cycles with a considerable stack ED of 367 Wh kg^{-1} was recorded.

2. Material and methods

2.1. Preparation of LNMO electrode

To fabricate LNMO electrode, $LiNi_{0.5}Mn_{1.5}O_4$ with $P4_332$ structure (LNMO, Guangdong Canrd New Energy Technology Co.,Ltd.), acetylene black (Alfa Aesar Co., Ltd.), and polyvinylidene fluoride (PVDF, Alfa Aesar Co., Ltd.) with a weight ratio of 94: 4: 2 in N-methyl pyrrolidinone (NMP, Sinopharm Chemical Reagent Co., Ltd.) were mixed in SK-300SII CE mixing machine (SHASHIN KAGAKU Co., Ltd.) for 20 min, producing a black slurry. Then, this slurry was spread on a clean Al foil by a doctor blade and dried at 60 °C for 12 h. The loaded foil was roll-pressed, and the mass of LNMO in this electrode is 10 mg cm^{-2} (half-cell) or 25 mg cm^{-2} (pouch cell) on average. Then, the 10 mg cm^{-2} electrode was punched into discs with a diameter of 14 mm, while the 25 mg cm^{-2} electrode was cut into 30 * 40 mm^2 plates.

2.2. Preparation of L_2NMO electrode

L_2NMO electrode was fabricated by chemical or electrochemical method. As for the chemical method, the as-prepared LNMO electrode and n-butyl-Li (1.6 M in hexanes, inno-chem Co., Ltd.) with a molar ratio of 1: 2 were mixed and reacted for 10 min and then washed with hexane for three times to obtain L_2NMO. L_2NMO electrode can also be fabricated by replacing n-butyl-Li with another lithiation agent, such as biphenyl-Li (2 m in DME) or naphthalene-Li (2 m in DME). As for the electrochemical method, super-thin Li foils (China Energy Lithium Co., Ltd.) were adhered to the LNMO electrodes by rolling, as illustrated in

Fig. S3. With the injection of electrolyte, Li foil and LNMO will generate L_{1+x}NMO spontaneously through an electrochemical reaction, x value can be controlled by the thickness of Li foil (5 −10 μm).

2.3. Preparation of half-cells and in-situ cell

LNMO and L_2NMO half-cells were assembled in CR2032-type coin cells using LNMO and L_2NMO as working electrodes and Li plate as counter electrodes, Celgard 3501 membrane as the separator, and 7 m bis(fluorosulfonyl)imide lithium (LiFSI) in fluoroethylene carbonate (FEC) as the electrolyte, which has wide enough electrochemical stability window, good compatibility with LNMO electrode, Al current collector corrosion resistance, and superior reversibility of LMA. The as-prepared half-cells were cycled in a voltage window of 3.3–4.85 V at 0.5C. The in-situ LNMO cell was assembled using a similar protocol but using an *in-situ* electrochemical cell.

2.4. Preparation of pouch cells

LNMO/Cu and L_2NMO/Cu pouch cells were assembled using LNMO and L_2NMO (30 * 40 mm^2) as the cathodes and Cu foils (31 * 41 mm^2) as anodes, Celgard 3501 membrane as the separator, 7 m LiFSI in FEC as electrolyte (2 g Ah^{-1}), and Al-plastic film as packaging.

2.5. Characterizations

The XRD measurements were conducted using a Bruker D8 ADVANCE diffractometer with Cu Kα radiation ($\lambda = 1.5405$ Å) in the scan range (2θ) of 10–70° An X-ray-transparent aluminum window was used for the in-situ measurements. The data for every single pattern was collected for 45 min with the scan range (2θ) of 17–50° The stoichiometry of LNMO and L_{1+x}NMO were obtained using an Inductive Coupled Plasma Emission Spectrometer (ICP, Thermo IRIS intrepid II). Scanning electron microscopy (SEM) images of the morphologies of LNMO and L_2NMO were taken by Hitachi S-4800 field emission scanning electron microscope, operated at 10 kV. Transmission electron microscopy (TEM) images of LNMO and L_2NMO were taken by JEOL JEM-2100 Plus transmission electron microscope, operated at 200 kV.

2.6. Electrochemical measurements

Galvanostatic cycling tests were conducted within a voltage window of 3.3–4.85 V (half-cells) or 3.3–4.8 V (pouch cells) using battery testers (Wuhan Land, China, and Neware, China) at 25 °C. The half-cells were cycled at 0.5C (1C = 146 mA g^{-1}). The pouch cells were charged to 4.8 V at 0.1C and held at 4.8 V until the anodic current dropped below 0.05C before being discharged to 3.3 V at 0.2C. For galvanostatic intermittent titration technique (GITT) measurement, the electrode was discharged/charged at a pulse current of 0.2C for a duration of 10 min, followed by a relaxation of 20 min at the open circuit to reach equilibrium potentials.

3. Results and discussion

3.1. Reversible phase transition between L_2NMO and LNMO

The reversible phase transition between L_2NMO and LNMO was confirmed in the LNMO/Li half-cells. The LNMO/Li cells can cycle reversibly in the different voltage ranges of 3.3–4.85 (LNMO ↔ NMO) and 1.9–4.85 V (L_2NMO ↔ LNMO ↔ NMO). Fig. S5 shows typical voltage profiles from 1.9 to 4.85 V at 0.2 C, where two low discharge plateaus appear at 2.7 and 2.0 V, indicating further lithiation of LNMO to generate L_2NMO. In the following charge process (Fig. S5), a new charge plateau appears at 2.9 V, originating from the Li-ion de-intercalation from L_2NMO, followed by the characteristic charge plateaus of LNMO at 4.0 and 4.7 V, proving that L_2NMO enables conversion back to LNMO reversibly. To further evaluate the mechanism of the reversible lithiation reaction of LNMO at 2.7 and 2.0 V, *in situ* X-ray diffraction (XRD) was performed to visually observe the discharge and charge process of LNMO. The *in situ* XRD test was performed for the discharge to 1.9 V and re-charge to 3.9 V at 0.1 C. Fig. 2a shows contour plots illustrating the evolution of the LNMO reflections whose corresponding XRD patterns are shown in Fig. S6. At first glance, all Bragg reflections of LNMO show good reversibility. Rietveld refinement of the XRD pattern at an open-circuit voltage (3.1 V) confirmed the sample to be of the spinel LNMO (Fig.s 2b and 2c)), which agrees with previous studies [8,48]. The refinement results are reported in Tab. S3. Notably, the characteristic (011), (013), (022), (004), and (123) reflections of spinel-related L_2NMO gradually appear as the discharge progressed, indicating continuous intercalation of Li-ions into the unoccupied LNMO octahedral sites without any structural damage. The tetrahedral Li-ions and the octahedral transition metal ions existing in LNMO still maintain in their original positions. Rietveld refinement of the XRD pattern collected from L_{1+x}NMO confirmed the coexistence of LNMO and L_2NMO (Fig. 2d). Then, with the further deepening of the discharge process, all the (111), (113), (222), and (133) reflections of spinel LNMO disappear, leaving only the L_2NMO reflections. Rietveld refinement of the XRD pattern discharged to 1.9 V confirmed the disappearance of LNMO (Fig. 2e), indicating the complete conversion of LNMO into L_2NMO. Next, during the subsequent charge process, the opposite evolution of the reflections can be observed. Once the voltage re-charges to 3.9 V, all the reflections of LNMO appeared again along with the disappearance of L_2NMO, revealing the reversible conversion between LNMO and L_2NMO.

The electron microscopy characterization shows that the morphology of LNMO is not affected by the lithiation process. Scanning electron microscope (SEM) images of LNMO and fully lithiated L_2NMO are shown in Fig. S7 and S8. Both samples are mixtures of microcrystals with particle sizes ranging from 1 to 5 μm, with no significant morphological changes between them, consistent with previous reports [46,47]. The insignificant volume expansion makes it possible to prepare L_2NMO electrodes by directly soaking the prepared LNMO electrodes in lithiation agents. The high-resolution transmission electron microscope (HRTEM) images of LNMO before and after lithiation with their corresponding selected area electron diffraction (SAED) (Fig. S9 and S10) also confirmed that LNMO reacted with n-butyl Li, forming L_2NMO. Notably, the chemical stability of L_2NMO stored in the air is also satisfactory (Fig. S11). Even exposed to air for five days, the reflections of L_2NMO do not degrade.

3.2. Electrochemical performance of L_2NMO in half-cells

Notably, the electrochemical conversion between LNMO and L_2NMO has an obvious potential hysteresis (Fig. 3a and S12) because Li-ions diffused rapidly through the unoccupied octahedral sites in LNMO, and the occupation of these sites during the formation of L_2NMO blocks the diffusion pathways of Li-ions. However, the EIS measurements show that even if the pathways are occupied, the Li-ions diffusion ability of L_2NMO is not affected (Fig. S13). Besides, the typical Jahn–Teller distortion owing to the generation of Mn^{3+} would have structural deformations if continuously cycled below 3 V (octahedral site). Thus, these octahedral sites are not suitable for energy storage due to limited kinetics and relatively low-working potential (< 2.8 V). However, it is ideal to use these octahedral sites as the Li reservoir once to offset the irreversible loss of Li on the anode side. To further prove that the one-time process after the release of the Li reservoir has no adverse effect on the electrochemical performance of AF-LMBs, an L_2NMO electrode was prepared by chemical lithiation, immersed in 1.6-M n-butyl Li solution for 10 min, and washed with hexane three times. After drying, the as-prepared L_2NMO electrode was paired with a Li plate to fabricate the half-cell. Compared with the LNMO cell, L_2NMO can release nearly twice Li resources during the first charge (Fig. 3b) by exhibiting an initial low CE of 45%. After acting as a Li reservoir, L_2NMO converts into normal LNMO and oper-

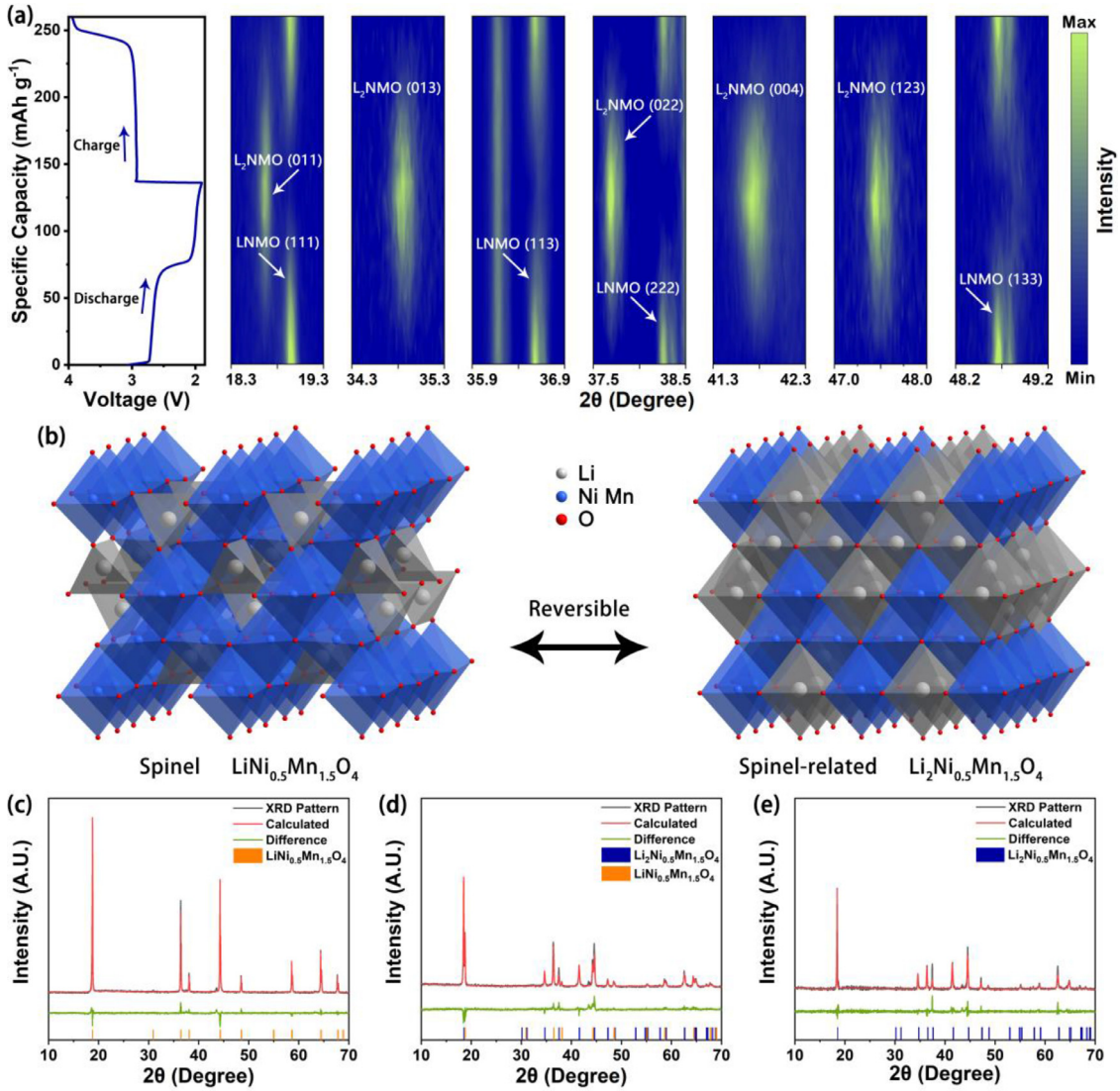

Fig. 2. Evaluation of the reversible phase transition between LNMO and L_2NMO. (a) Contour plot of *in situ* XRD patterns of an LNMO half-cell and corresponding voltage profiles. (b) Crystal structures of LNMO and L_2NMO. XRD patterns, along with the corresponding Rietveld refinements of (c) LNMO, (d) L_{1+x}NMO, and (e) L_2NMO.

ates under a voltage window of 3.3–4.85 V. Notably. However, working under the same conditions, the L_2NMO electrode exhibits a higher initial discharge capacity of 129 mAh g^{-1} (Fig. 3b), which probably results from the activation of the cathode material by the formation of the Li-rich phase. Besides, the voltage profiles of L_2NMO and LNMO at the second cycle coincide perfectly (Fig. 3c), proving that the formation of the Li-rich phase does not affect the stability of LNMO. The cyclic voltammetry (CV) curves of LNMO and L_2NMO cells in the initial cycles confirmed the reversible phase transition between LNMO and L_2NMO again (Fig. S14). After removing the Li reservoir, L_2NMO converts back to its original spinel structure, operating under a high voltage of 4.7 V. The cycling stability and rate capability of L_2NMO after releasing the Li resources was verified further (Fig. 3d and S15). The L_2NMO cell shows the same CR as that of the LNMO cell after 100 cycles, indicating that L_2NMO is a promising cathode material for AF-LMBs, providing twice-active Li supplementation without sacrificing its cycling stability. And the L_2NMO cell even shows better rate capability at higher current density, which is due to the different Li morphologies on the anode side. After the first cycle, the L_2NMO cell will produce nearly twice as much plated Li on the anode side, which has a larger surface area than bulk Li and better kinetics at a high rate, thus achieving higher capacity.

3.3. Electrochemical performance of L_2NMO anode-free pouch cells

To further confirm our abovementioned claims, L_2NMO was applied in AF-LMBs, where the anode faces more challenges due to its low CE. The 80-mAh level multi-layer anode-free pouch cells were assembled with L_2NMO and LNMO as cathodes (25 mg cm^{-2} and 30 mm × 40 mm in dimension) and Cu foils (31 mm × 41 mm in dimension) as anodes, respectively (Please see the detailed parameters of the pouch cell in Fig. 4a and S16 and Tab. S4–S6). Owing to the anode-free design, the stack ED of the multi-layer L_2NMO/Cu cell reaches 367 Wh kg^{-1} (Fig. S17), which outperformance many reported Co-free AF-LMBs (Tab. S7) [18,50-57]. Fig. 4b shows that the L_2NMO/Cu exhibits a higher initial specific capacity of 128 mAh g^{-1}, with a higher CR of 88% after 50 cycles compared to that of LNMO/Cu (120 mAh g^{-1} and 39%). Due to the adequate Li supplements in L_2NMO, L_2NMO/Cu can accumulate excess active Li on the anode side as the Li reservoir after the first cycle (Fig. S18 and S19), as shown in the first cycle voltage profiles of LNMO/Cu and L_2NMO/Cu pouch cells (Fig. 4c). Compared with the LNMO/Cu cell, L_2NMO/Cu displays a new plateau at 2.9 V in the charge corresponding to the transfer of active Li from the L_2NMO cathode to the anode, resulting in a higher charge capacity of 265 mAh g^{-1}. The amount of active Li in LNMO/Cu

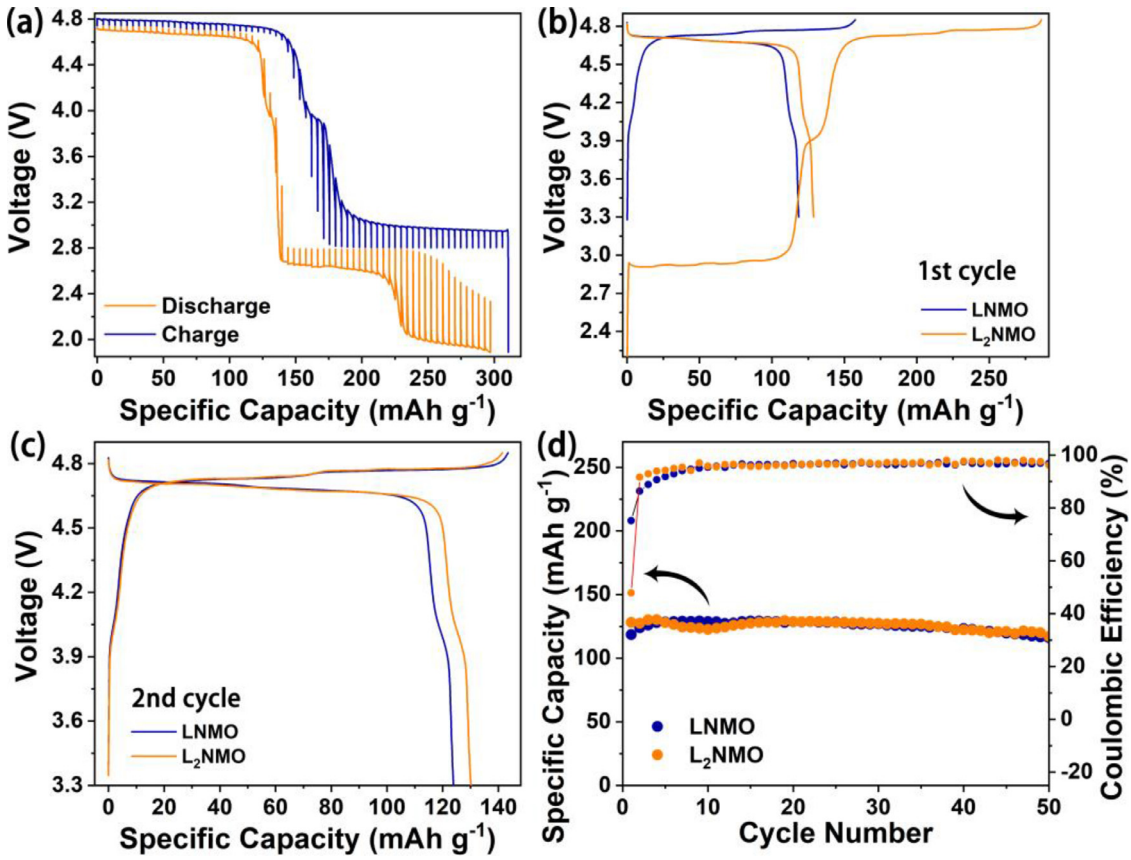

Fig. 3. Electrochemical performance of L_2NMO cathode. (a) Quasi-equilibrium voltage profile of LNMO (discharged from 4.8 to 1.9 V and then re-charged to 4.8 V) obtained from galvanostatic intermittent titration technique (GITT) in the half-cell. Voltage profiles of LNMO and L_2NMO half-cell for the (b) first and (c) second cycles. (d) Cycling performances of LNMO and L_2NMO half-cells.

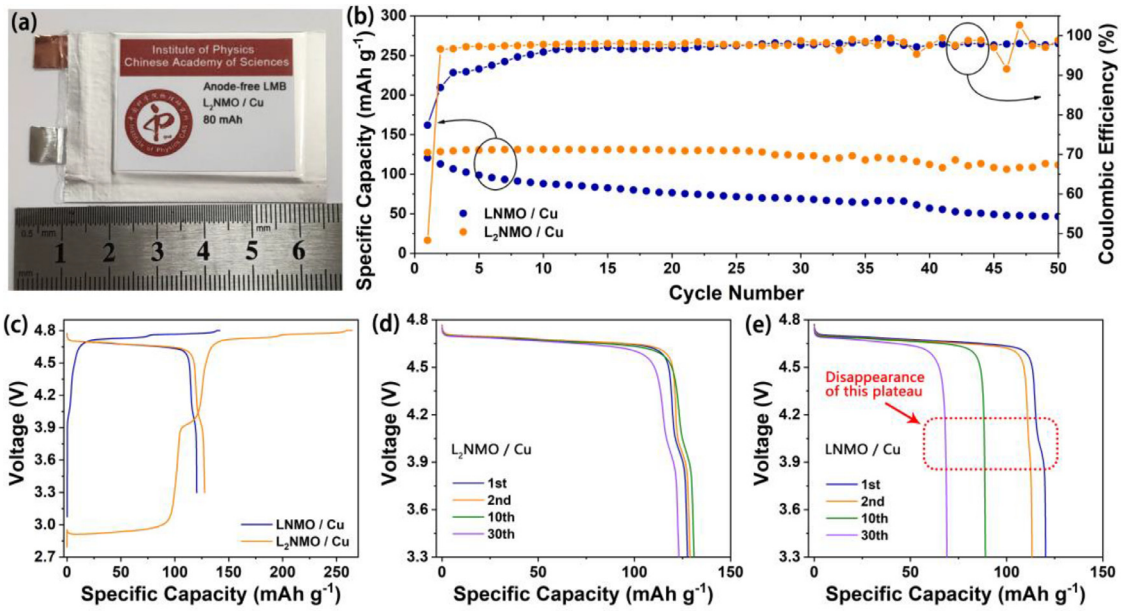

Fig. 4. Demonstration of anode-free L_2NMO pouch cells. (a) Picture of the 80-mAh level multi-layer anode-free pouch cell. (b) Cycling performances of LNMO/Cu and L_2NMO/Cu pouch cells. (c) Voltage profiles of LNMO/Cu and L_2NMO/Cu pouch cells for the first cycle. Voltage profiles of (d) L_2NMO/Cu and (e) LNMO/Cu pouch cells for different cycles. (The pouch cells were charged at 0.1 C and discharged at 0.2 C).

and L_2NMO/Cu cells were determined by redepositing the plated Li to another Cu foil (Fig. S20). The active Li in L_2NMO/Cu cell is nearly twice as much as that in LNMO cell. The extra active Li continuously offsets the irreversible loss of Li in the following cycles, thereby extending the lifespan of the battery, like a disposable fuel tank for a space shuttle. Therefore, the CEs of L_2NMO/Cu cell after the formation cycle are significantly higher than those of LNMO/Cu cell, especially in the first ten cycles (Fig. 4b). And the L_2NMO/Cu cell cycles stably without visible capacity loss during the following 50 cycles.

Fig. 4d shows the discharge voltage profiles of L_2NMO/Cu pouch cells at the 1st, 2nd, 10th, and 30th cycles, where all the curves coincide well, with no visible voltage fading even after 30 cycles. In comparison, the capacity of the LNMO/Cu cell fades rapidly throughout its cycling, with the disappearance of its second discharge plateau at 3.9 V (Fig. 4e). Notably, the disappearance of the second plateau or not is determined by different mechanisms in cell decay. Due to the formation of the initial Li reservoir in the L_2NMO cell, the capacity ratio of the anode to cathode (A/C) is >1, and the cathode is the limiting electrode [58]. Even after 30 cycles, enough anode material can still ensure the complete Li intercalation into the cathode (the appearance of intact 3.9 V plateau), and the slight decline in cell capacity is due to the cathode degradation (Fig. 4d). For the LNMO cell, although its A/C ratio was initially ~1, severe irreversible Li loss from the anode side results in an A/C ratio of < 1. After the first cycle, the anode capacity is unable to support the entire release of the cathode capacity, resulting in the disappearance of the 3.9-V plateau (Fig. 4e).

4. Conclusions

The Co resource restriction issue promotes the demand for Co-free high ED batteries. 5 V class anode-free Li metal battery with spinel-related $Li_2Ni_{0.5}Mn_{1.5}O_4$ (L_2NMO) cathode can meet such a requirement by providing considerable ED and improving lifespan. In the first charge process, the Li-rich L_2NMO first acts as a Li donor to release an extra Li-ions, which supplements the Li loss in the anode. Afterward, it functions as a high voltage LNMO cathode, accumulating an appropriate amount of Li reservoir without affecting the thick Li foil at the expense of the ED. Using L_2NMO, the multi-layer anode-free pouch cell attains a stack ED of 367 Wh kg^{-1} and CR above 88% after 50 cycles under high cathode mass loading (25 mg cm^{-2}) and limited electrolyte addition (E/C ratio of 2 g Ah^{-1}). All these abovementioned advantages make this strategy attractive to the broader price-sensitive markets, which also pursue high ED.

Declaration of Competing Interest

The authors declare that they have no known competing financial interests or personal relationships that could have appeared to influence the work reported in this paper.

CRediT authorship contribution statement

Liangdong Lin: Methodology, Investigation, Writing – original draft, Funding acquisition. **Kun Qin:** Investigation, Resources. **Meiying Li:** Investigation. **Yong-sheng Hu:** Supervision, Funding acquisition. **Hong Li:** Supervision, Funding acquisition. **Xuejie Huang:** Supervision, Funding acquisition. **Liquan Chen:** Supervision, Funding acquisition. **Liumin Suo:** Supervision, Writing – review & editing, Project administration, Funding acquisition.

Acknowledgments

This work is supported by the Center for Clean Energy. L. Lin acknowledges China Postdoctoral Science Foundation (2019M660845).

Supplementary materials

Supplementary material associated with this article can be found, in the online version, at doi:10.1016/j.ensm.2021.12.036.

References

[1] M. Armand, J.M. Tarascon, Nature 451 (2008) 652–657.
[2] B. Dunn, H. Kamath, J.-M. Tarascon, Science 334 (2011) 928.
[3] J.W. Choi, D. Aurbach, Nat. Rev. Mater. 1 (2016) 16013.
[4] L. Wang, B. Chen, J. Ma, G. Cui, L. Chen, Chem. Soc. Rev. 47 (2018) 6505–6602.
[5] M. Li, J. Lu, Science 367 (2020) 979.
[6] N. Li, S. Sallis, J.K. Papp, B.D. McCloskey, W. Yang, W. Tong, Nano Energy 78 (2020) 105365.
[7] Z. Yang, L. Mu, D. Hou, M.M. Rahman, Z. Xu, J. Liu, D. Nordlund, C.-J. Sun, X. Xiao, F. Lin, Adv. Energy Mater. 11 (2021) 2002719.
[8] S.H. Park, S.W. Oh, S.H. Kang, I. Belharouak, K. Amine, Y.K. Sun, Electrochim. Acta 52 (2007) 7226–7230.
[9] L. Suo, W. Xue, M. Gobet, S.G. Greenbaum, C. Wang, Y. Chen, W. Yang, Y. Li, J. Li, Proc. Natl. Acad. Sci. U. S. A. 115 (2018) 1156.
[10] M.S. Whittingham, Chem. Rev. 104 (2004) 4271–4302.
[11] T. Ohzuku, J. Electrochem. Soc. 140 (1993) 1862.
[12] N.N. Bramnik, K.G. Bramnik, T. Buhrmester, C. Baehtz, H. Ehrenberg, H. Fuess, J. Solid State Electrochem. 8 (2004) 558–564.
[13] C. Liu, Z.G. Neale, G. Cao, Mater. Today 19 (2016) 109–123.
[14] N. Kuwata, S. Kudo, Y. Matsuda, J. Kawamura, Solid State Ionics 262 (2014) 165–169.
[15] Y.-K. Sun, S.-T. Myung, M.-H. Kim, J. Prakash, K. Amine, J. Am. Chem. Soc. 127 (2005) 13411–13418.
[16] M.-H. Kim, H.-S. Shin, D. Shin, Y.-K. Sun, J. Power Sources 159 (2006) 1328–1333.
[17] S. Nanda, A. Gupta, A. Manthiram, Adv. Energy Mater. 11 (2020) 2000804.
[18] J. Qian, B.D. Adams, J. Zheng, W. Xu, W.A. Henderson, J. Wang, M.E. Bowden, S. Xu, J. Hu, J.-G. Zhang, Adv. Funct. Mater. 26 (2016) 7094–7102.
[19] A.J. Louli, A. Eldesoky, R. Weber, M. Genovese, M. Coon, J. deGooyer, Z. Deng, R.T. White, J. Lee, T. Rodgers, R. Petibon, S. Hy, S.J.H. Cheng, J.R. Dahn, Nat. Energy 5 (2020) 693–702.
[20] R. Weber, M. Genovese, A.J. Louli, S. Hames, C. Martin, I.G. Hill, J.R. Dahn, Nat. Energy 4 (2019) 683–689.
[21] Z. Yu, H. Wang, X. Kong, W. Huang, Y. Tsao, D.G. Mackanic, K. Wang, X. Wang, W. Huang, S. Choudhury, Y. Zheng, C.V. Amanchukwu, S.T. Hung, Y. Ma, E.G. Lomeli, J. Qin, Y. Cui, Z. Bao, Nat. Energy 5 (2020) 526–533.
[22] P. Albertus, S. Babinec, S. Litzelman, A. Newman, Nat. Energy 3 (2018) 16–21.
[23] D. Lin, Y. Liu, Y. Cui, Nat. Nanotechnol. 12 (2017) 194–206.
[24] N. Li, Y. Shi, Y.X. Yin, X. Zeng, Y. Guo, Angew. Chem. Int. Ed. 57 (2018) 1505–1509.
[25] L. Lin, F. Liang, K. Zhang, H. Mao, J. Yang, Y. Qian, J. Mater. Chem. A 6 (2018) 15859–15867.
[26] H. Ye, Z. Zheng, H. Yao, S. Liu, T. Zuo, X. Wu, Y. Yin, N. Li, J. Gu, F. Cao, Y. Guo, Angew. Chem. Int. Ed. 58 (2019) 1094–1099.
[27] L. Lin, J. Wang, R. Li, C. Wang, C. Zhang, J. Yang, Y. Qian, Energy Storage Mater 26 (2020) 112–118.
[28] S.S. Zhang, ACS Appl. Energy Mater. 1 (2018) 910–920.
[29] S. Chen, J. Zheng, D. Mei, K.S. Han, M.H. Engelhard, W. Zhao, W. Xu, J. Liu, J.-G. Zhang, Adv. Mater. 30 (2018) 1706102.
[30] Y. Yang, D.M. Davies, Y. Yin, O. Borodin, J.Z. Lee, C. Fang, M. Olguin, Y. Zhang, E.S. Sablina, X. Wang, C.S. Rustomji, Y.S. Meng, Joule 3 (2019) 1986–2000.
[31] X. Cao, X. Ren, L. Zou, M.H. Engelhard, W. Huang, H. Wang, B.E. Matthews, H. Lee, C. Niu, B.W. Arey, Y. Cui, C. Wang, J. Xiao, J. Liu, W. Xu, J.-G. Zhang, Nat. Energy 4 (2019) 796–805.
[32] C. Yan, H.-R. Li, X. Chen, X.-Q. Zhang, X.-B. Cheng, R. Xu, J.-Q. Huang, Q. Zhang, J. Am. Chem. Soc. 141 (2019) 9422–9429.
[33] L. Lin, L. Suo, Y.-S. Hu, H. Li, X. Huang, L. Chen, Adv. Energy Mater. 11 (2021) 2003709.
[34] K.-H. Chen, A.J. Sanchez, E. Kazyak, A.L. Davis, N.P. Dasgupta, Adv. Energy Mater. 9 (2019) 1802534.
[35] L. Lin, K. Qin, Q. Zhang, L. Gu, L. Suo, Y.-s. Hu, H. Li, X. Huang, L. Chen, Angew. Chem. Int. Ed. 60 (2021) 8289–8296.
[36] W.I.F. David, M.M. Thackeray, L.A. De Picciotto, J.B. Goodenough, J. Solid State Chem. 67 (1987) 316–323.
[37] H. Li, G. Richter, J. Maier, Adv. Mater. 15 (2003) 736–739.
[38] H. Lee, S.-K. Chang, E.-Y. Goh, J.-Y. Jeong, J.H. Lee, H.-J. Kim, J.-J. Cho, S.-T. Hong, Chem. Mater. 20 (2008) 5–7.
[39] D. Shanmukaraj, S. Grugeon, S. Laruelle, G. Douglade, J.-M. Tarascon, M. Armand, Electrochem. Commun. 12 (2010) 1344–1347.
[40] M.G. Kim, J. Cho, J. Mater. Chem. 18 (2008) 5880–5887.
[41] X. Su, C. Lin, X. Wang, V.A. Maroni, Y. Ren, C.S. Johnson, W. Lu, J. Power Sources 324 (2016) 150–157.
[42] J. Du, W. Wang, A.Y. Sheng Eng, X. Liu, M. Wan, Z.W. Seh, Y. Sun, Nano Lett 20 (2020) 546–552.
[43] J. Zhao, Z. Lu, N. Liu, H.-W. Lee, M.T. McDowell, Y. Cui, Nat. Commun. 5 (2014) 5088.
[44] P. Poizot, S. Laruelle, S. Grugeon, L. Dupont, J.M. Tarascon, Nature 407 (2000) 496–499.
[45] Z. Moorhead-Rosenberg, E. Allcorn, A. Manthiram, Chem. Mater. 26 (2014) 5905–5913.

[46] M. Mancini, P. Axmann, G. Gabrielli, M. Kinyanjui, U. Kaiser, M. Wohlfahrt-Mehrens, ChemSusChem 9 (2016) 1843–1849.
[47] G. Gabrielli, M. Marinaro, M. Mancini, P. Axmann, M. Wohlfahrt-Mehrens, J. Power Sources 351 (2017) 35–44.
[48] M. Mancini, G. Gabrielli, P. Axmann, M. Wohlfahrt-Mehrens, J. Electrochem. Soc. 164 (2016) A6229–A6235.
[49] W.M. Dose, J. Blauwkamp, M.J. Piernas-Muñoz, I. Bloom, X. Rui, R.F. Klie, P. Senguttuvan, C.S. Johnson, ACS Appl. Energy Mater. 2 (2019) 5019–5028.
[50] Z.L. Brown, S. Jurng, B.L. Lucht, J. Electrochem. Soc. 164 (2017) A2186–A2189.
[51] S. Nanda, A. Gupta, A. Manthiram, Adv. Energy Mater. 8 (2018) 1801556.
[52] A.A. Assegie, J.-H. Cheng, L.-M. Kuo, W.-N. Su, B.-J. Hwang, Nanoscale 10 (2018) 6125–6138.
[53] A.A. Assegie, C.-C. Chung, M.-C. Tsai, W.-N. Su, C.-W. Chen, B.-J. Hwang, Nanoscale 11 (2019) 2710–2720.
[54] T.T. Beyene, H.K. Bezabh, M.A. Weret, T.M. Hagos, C.-J. Huang, C.-H. Wang, W.-N. Su, H. Dai, B.-J. Hwang, J. Electrochem. Soc. 166 (2019) A1501–A1509.
[55] Z.L. Brown, S. Heiskanen, B.L. Lucht, J. Electrochem. Soc. 166 (2019) A2523–A2527.
[56] T.T. Beyene, B.A. Jote, Z.T. Wondimkun, B.W. Olbassa, C.-J. Huang, B. Thirumalraj, C.-H. Wang, W.-N. Su, H. Dai, B.-J. Hwang, ACS Appl. Mater. Interfaces 11 (2019) 31962–31971.
[57] V. Nilsson, A. Kotronia, M. Lacey, K. Edström, P. Johansson, ACS Appl. Energy Mater. 3 (2020) 200–207.
[58] C.-J. Huang, B. Thirumalraj, H.-C. Tao, K.N. Shitaw, H. Sutiono, T.T. Hagos, T.T. Beyene, L.-M. Kuo, C.-C. Wang, S.-H. Wu, W.-N. Su, B.J. Hwang, Nat. Commun. 12 (2021) 1452.